Appl. Math. Mech. -Engl. Ed., **39**(10), 1485–1498 (2018)

Applied Mathematics and Mechanics (English Edition)

https://doi.org/10.1007/s10483-018-2372-8

Revisiting the elastic solution for an inner-pressured functionally graded thick-walled tube within a uniform magnetic field*

Libiao XIN[1,2,†], Yanbin LI[3], Dongmei PAN[4], Guansuo DUI[5], Chengjian JU[5]

1. Shanxi Key Laboratory of Material Strength & Structural Impact, College of Mechanics, Taiyuan University of Technology, Taiyuan 030024, China;
2. National Demonstration Center for Experimental Mechanics Education, College of Mechanics, Taiyuan University of Technology, Taiyuan 030024, China;
3. Applied Mechanics of Materials Laboratory, Department of Mechanical Engineering, Temple University, Philadelphia, Pennsylvania 19122, U. S. A.;
4. Department of Civil and Environmental Engineering, University of Houston, Houston, Texas 77204, U. S. A.;
5. Institute of Mechanics, Beijing Jiaotong University, Beijing 100044, China

(Received Apr. 14, 2018 / Revised Jun. 18, 2018)

Abstract In this paper, the mechanical responses of a thick-walled functionally graded hollow cylinder subject to a uniform magnetic field and inner-pressurized loads are studied. Rather than directly assume the material constants as some specific function forms displayed in pre-studies, we firstly give the volume fractions of different constituents of the functionally graded material (FGM) cylinder and then determine the expressions of the material constants. With the use of the Voigt method, the corresponding analytical solutions of displacements in the radial direction, the strain and stress components, and the perturbation magnetic field vector are derived. In the numerical part, the effects of the volume fraction on the displacement, strain and stress components, and the magnetic perturbation field vector are investigated. Moreover, by some appropriate choices of the material constants, we find that the obtained results in this paper can reduce to some special cases given in the previous studies.

Key words functionally graded material (FGM), thick-walled tube, elasticity solution, magnetic field, perturbation of magnetic field vector

Chinese Library Classification O343.1
2010 Mathematics Subject Classification 74E30, 74M25

* Citation: XIN, L. B., LI, Y. B., PAN, D. M., DUI, G. S., and JU, C. J. Revisiting the elastic solution for an inner-pressured functionally graded thick-walled tube within a uniform magnetic field. *Applied Mathematics and Mechanics* (*English Edition*), **39**(10), 1485–1498 (2018) https://doi.org/10.1007/s10483-018-2372-8

† Corresponding author, E-mail: xinlibiao@tyut.edu.cn

Project supported by the National Natural Science Foundation of China (No. 11772041)

1 Introduction

In the last several decades, functionally graded materials (FGMs) have been thoroughly investigated because of their ability to optimize mechanical behaviors by setting the material parameters as some unique functional forms. Therefore, with such attractive and practical advantages, FGMs have been widely applied into various fields, such as the energy conversion fields, transportation, model-cutting tools, surface wrinkling, semiconductors manufacture and bio-systems[1–5]. Zheng et al.[6] systematically studied the laterally variable thickness (LVT) multi-cell tubes for crashworthiness. The optimization problem of crashworthiness of automotive parts with the tailor rolled blank was investigated by Sun et al.[7]. For the energy absorption of thin-walled structures, Sun et al.[8] introduced the functionally graded thin-walled structures and investigated the crashworthiness subject to an axial crushing load.

As for the FGM vessels under various loading conditions, there have been a large number of researchers exploring its elastic and elastoplastic responses with different methods[9–15]. By functionalizing the elastic modulus as an exponential form in the radial direction, You et al.[9] obtained the exact elastic expressions of stress components and the radial displacement of an inner-pressurized FGM cylinder. By using a power-function-form Young's modulus and keeping Poisson's ratio constant, Tutuncu and Ozturk[10] analyzed the elastic behaviors of FGM vessels with mechanical loadings. With a linear function form of elastic modulus, Shi et al.[11] gave the elastic results of the problem, which is the same as that in Ref. [10].

The above works merely focus on the problems subject to mechanical loads. Smart materials with piezomagnetic and piezoelectric effects as well as magnetoelectricity can be often exposed to mechanical, electric, and magnetic fields[16–28], in which the coupling effect can be a candidate for tailoring intelligent structures with numerous utilization such as the large actuation and the energy harvesting[26–28]. For example, researchers[29–34] have studied the effects of magnetic field on the elastic constants of magnetic elastomers and found that the material becomes stiffer in a magnetic field. Therefore, by this way, it is rather vital and necessary to have a better understanding of the impacts of magnetic field on the materials mechanical behaviors, especially for the FGMs specializing material properties purposely by the variation of material parameters.

Recently, by assuming the elastic modulus and magnetic permeability as power series forms (for example, by setting $\mu(r) = \mu_0 r^\beta$ and $E(r) = E_0 r^\beta$) along the concerned directions, the analytical results of both displacements and the components of stresses and strains have been derived correspondingly when dealing with the inner pressurized FGM hollow cylinder problems[35–42]. For the same problem, some other situations like Young's modulus denoted by an exponential function form while the magnetic permeability was assumed as constant were thoroughly researched[43–46]. However, all these works ignored the effect of Poisson's ratio which has been reflected by analyzing the radial displacements and stress components of the mechanical loaded FGM tubes under a uniform magnetic field[47–48]. Furthermore, the FGMs can be literally and theoretically considered to be composed by grading its different components in certain directions by some specific volume fraction forms. However, if the expressions of the components' volume fractions are set with inappropriate forms, rather complex mathematical derivation efforts and complicated results originate[49]. Acknowledging this fact, in this paper, we define the volume fraction of each phase of the FGMs as an exponential form with three variables (the same as Refs. [48] and [50]) which can keep consistent with the patterns presented in lots of previous works merely by adjusting these three indexes.

In this work, we have studied the inner pressurized FGM tubes in uniform magnetic fields. In Section 2, the theoretical derivation works are finished with the analytical results of the radial displacement, stress components, and the perturbation magnetic field vector. Then, the effects of Poisson's ratio, the magnetic intensity, and the parameter n in the volume fraction function are discussed in Section 3. Finally, Section 4 gives some conclusions.

2 Theoretical analyses

The configuration of an inner pressurized FGM tube under uniform magnetic fields within the cylindrical polar coordinate (r, θ, z) is displayed in Fig. 1, and the stress boundary conditions are $\sigma_r|_{r=a} = -p$ and $\sigma_r|_{r=b} = 0$ (a and b are the inner and outer radii, respectively). In this paper, the FGM tube consists of two distinct materials A and B, and the volume fraction of material A is assumed to vary in the radial direction with an expression as

$$c(r) = c_0 + c_1(r/b)^n, \tag{1}$$

where c_0, c_1, and n are three material parameters.

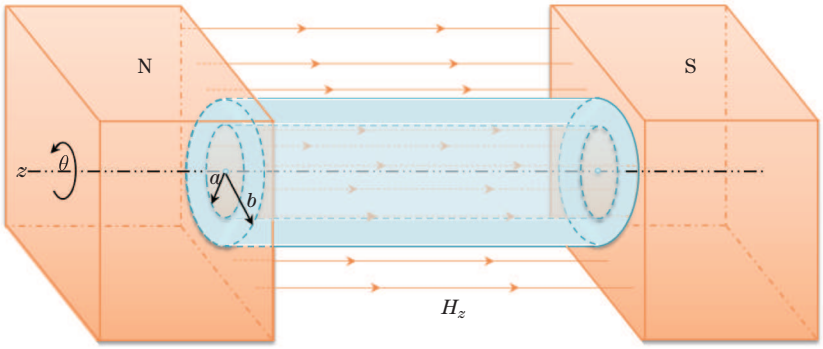

Fig. 1 A schematic diagram of a long FGM tube subject to an internal pressure in a uniform magnetic field H_z

The average stress and strain in a representative volume element (RVE) V can be defined as[51–53]

$$\begin{cases} \sigma = \dfrac{1}{V}\displaystyle\int_V \widehat{\sigma}(x)\mathrm{d}x, \quad \varepsilon = \dfrac{1}{V}\int_V \widehat{\varepsilon}(x)\mathrm{d}x, \\ \sigma^{(i)} = \dfrac{1}{V_i}\displaystyle\int_{V_i} \widehat{\sigma}^{(i)}(x)\mathrm{d}x, \quad \varepsilon^{(i)} = \dfrac{1}{V_i}\int_{V_i} \widehat{\varepsilon}^{(i)}(x)\mathrm{d}x, \end{cases} \tag{2}$$

where $\widehat{\sigma}$ and $\widehat{\varepsilon}$ are the stress and strain fields over the RVE, respectively, $\widehat{\sigma}^{(i)}$ and $\widehat{\varepsilon}^{(i)}$ are the constituents, σ and ε are the overall volume average stress and strain of the RVE, respectively, and $\sigma^{(i)}$ and $\varepsilon^{(i)}$ are the components with the volume V_i.

For the case in this paper, with the Voigt method and uniform strain field assumption, the stress and strain can be respectively expressed as

$$\sigma = c(r)\sigma^{(1)} + (1 - c(r))\sigma^{(2)}, \tag{3}$$

$$\varepsilon_\theta^{(1)} = \varepsilon_\theta^{(2)} = \varepsilon_\theta, \quad \varepsilon_r^{(1)} = \varepsilon_r^{(2)} = \varepsilon_r, \tag{4}$$

where $i = 1$ and 2 denote the materials A and B, respectively, $\sigma^{(1)}$ and $\sigma^{(2)}$ are the average stresses of the materials A and B, respectively, and $\varepsilon_r^{(i)}$ and $\varepsilon_\theta^{(i)}$ represent the radial and circumferential strains, respectively.

For the linear elastic deformation, we have

$$\varepsilon_r = \frac{\mathrm{d}u}{\mathrm{d}r}, \quad \varepsilon_\theta = \frac{u}{r}, \tag{5}$$

where u stands for the radial displacement. For each component of the FGM tube, Hooke's law can be written as

$$\begin{cases} \sigma_r^{(i)} = \lambda_i \varepsilon_\theta^{(i)} + (\lambda_i + 2G_i)\varepsilon_r^{(i)}, \\ \sigma_\theta^{(i)} = (\lambda_i + 2G_i)\varepsilon_\theta^{(i)} + \lambda_i \varepsilon_r^{(i)}, \\ \sigma_z^{(i)} = \lambda_i(\varepsilon_\theta^{(i)} + \varepsilon_r^{(i)}), \end{cases} \tag{6}$$

where λ_i and G_i are the Lamé constants, and $\sigma_r^{(i)}$, $\sigma_\theta^{(i)}$, and $\sigma_z^{(i)}$ are the stress components in the radial, circumferential, and axial directions, respectively.

Substituting Eq. (6) into Eq. (3) gives the average stress components of the FGM tube,

$$\begin{cases} \sigma_r = \overline{\lambda}\dfrac{u}{r} + (\overline{\lambda} + 2\overline{G})\dfrac{\mathrm{d}u}{\mathrm{d}r}, \\ \sigma_\theta = (\overline{\lambda} + 2\overline{G})\dfrac{u}{r} + \overline{\lambda}\dfrac{\mathrm{d}u}{\mathrm{d}r}, \\ \sigma_z = \overline{\lambda}\Big(\dfrac{u}{r} + \dfrac{\mathrm{d}u}{\mathrm{d}r}\Big), \end{cases} \tag{7}$$

where

$$\begin{cases} \overline{\lambda} = c(r)\lambda_1 + (1 - c(r))\lambda_2, \\ \overline{G} = c(r)G_1 + (1 - c(r))G_2. \end{cases} \tag{8}$$

With the following assumptions: (a) each material component of the FGM tube is non-ferromagnetic and non-ferroelectric; (b) the Thompson effects are omittable; (c) the displacement electric currents are ignored, for the elastic medium with perfect conductions, the simplified electrodynamics, Maxwell's equations can be written as[41–42]

$$\begin{cases} \boldsymbol{J} = \nabla \times \boldsymbol{h}, \quad \boldsymbol{h} = \nabla \times (\boldsymbol{U} \times \boldsymbol{H}), \quad \operatorname{div} \boldsymbol{h} = 0, \\ \boldsymbol{e} = -\mu(r)\Big(\dfrac{\partial \boldsymbol{U}}{\partial t} \times \boldsymbol{H}\Big), \quad \nabla \times \boldsymbol{e} = -\mu(r)\dfrac{\partial \boldsymbol{h}}{\partial t}, \end{cases} \tag{9}$$

where $\boldsymbol{J}, \boldsymbol{h}, \boldsymbol{U}, \boldsymbol{H}, \boldsymbol{e}$, and t are the electric current density, the perturbation of magnetic field, the displacement vector, the magnetic intensity, the perturbation of electric field vector, and the time variable, respectively.

Taking the initial magnetic field vector $\boldsymbol{H}\,(0, 0, H_z)$ into Eq. (9) yields

$$\begin{cases} \boldsymbol{U} = (u, 0, 0), \quad \boldsymbol{e} = \mu(r)\Big(0, H_z\dfrac{\partial u}{\partial t}, 0\Big), \quad \boldsymbol{h} = (0, 0, h_z), \\ \boldsymbol{J} = \Big(0, -\dfrac{\partial h_z}{\partial r}, 0\Big), \quad h_z = -H_z\Big(\dfrac{\partial u}{\partial r} + \dfrac{u}{r}\Big). \end{cases} \tag{10}$$

Then, with $\boldsymbol{f} = \mu(r)\,(\boldsymbol{J} \times \boldsymbol{H})$, the radial Lorentz's stress f_r can be induced as

$$f_r = H_z^2 \mu(r)\Big(\frac{\partial^2 u}{\partial r^2} + \frac{1}{r}\frac{\partial u}{\partial r} - \frac{u}{r^2}\Big), \tag{11}$$

where $\mu(r)$, the magnetic permeability of the FGM tube, can be expressed with the Voigt method as

$$\mu(r) = c(r)\mu_1 + (1 - c(r))\mu_2. \tag{12}$$

Substituting Eqs. (7), (11), and (12) into the equilibrium equation, i.e.,

$$\frac{\mathrm{d}\sigma_r}{\mathrm{d}r}+\frac{\sigma_r-\sigma_\theta}{r}+f_r=0, \tag{13}$$

yields the governing ordinary differential equation for the radial displacement u,

$$r(\phi_1-\phi_2 r^n)\frac{\mathrm{d}^2u}{\mathrm{d}r^2}+(\phi_1-\phi_3 r^n)\frac{\mathrm{d}u}{\mathrm{d}r}-(\phi_1+\phi_4 r^n)\frac{u}{r}=0, \tag{14}$$

where

$$\begin{cases}\phi_1=c_0(\lambda_1+2G_1+\mu_1H_z^2)+(1-c_0)(\lambda_2+2G_2+\mu_2H_z^2),\\ \phi_2=c_1(\lambda_2+2G_2+\mu_2H_z^2-\lambda_1-2G_1-\mu_1H_z^2)/b^n,\\ \phi_3=(n+1)\phi_2+c_1nH_z^2(\mu_1-\mu_2)/b^n,\\ \phi_4=n(\lambda_2-\lambda_1)c_1/b^n-\phi_2.\end{cases} \tag{15}$$

2.1 Case 1: $\phi_1 \neq 0$

For the case $\phi_1 \neq 0$, Eq. (14) can be rearranged as

$$r\Big(1-\frac{\phi_2}{\phi_1}r^n\Big)\frac{\mathrm{d}^2u}{\mathrm{d}r^2}+\Big(1-\frac{\phi_3}{\phi_1}r^n\Big)\frac{\mathrm{d}u}{\mathrm{d}r}-\Big(1+\frac{\phi_4}{\phi_1}r^n\Big)\frac{u}{r}=0. \tag{16}$$

For convenience, by setting $x=\chi(r)=\frac{\phi_2}{\phi_1}r^n$, Eq. (16) can be rewritten as

$$x^2(1-x)\frac{\mathrm{d}^2u}{\mathrm{d}x^2}+x\Big(1-\frac{n-1+\phi_3/\phi_2}{n}x\Big)\frac{\mathrm{d}u}{\mathrm{d}x}-\frac{1}{n^2}\Big(1+\frac{\phi_4}{\phi_2}x\Big)u=0. \tag{17}$$

According to Ref. [54], Eq. (17) can be solved as

$$u(r)=C_1rF(\alpha,\beta,\delta;x)+C_2\frac{1}{r}F(\alpha-\delta+1,\beta-\delta+1,2-\delta;x), \tag{18}$$

where C_1 and C_2 are constants, and F is the hypergeometric function defined in $|x|<1$ with a power series form as

$$F(\alpha,\beta,\delta;x)=1+\sum_{m=1}^{\infty}\frac{C_{\alpha+m-1}^mC_{\beta+m-1}^m}{C_{\delta+m-1}^m}x^m, \tag{19}$$

in which

$$\delta=1+\frac{2}{n},\quad \alpha=\frac{\sqrt{(\phi_3/\phi_2-1)^2-4\phi_4/\phi_2}+\phi_3/\phi_2+1}{2n},\quad \beta=\frac{\phi_3/\phi_2+1}{n}-\alpha. \tag{20}$$

Note that Eq. (18) holds throughout by the following. Rearrange the radial displacement

$$u(r)=C_1P(r)+C_2Q(r), \tag{21}$$

where the specific forms of $P(r)$ and $Q(r)$ and their derivatives with respect to r are

$$\begin{cases}P(r)=rF(\alpha,\beta,\delta;x),\\ Q(r)=\dfrac{1}{r}F(\alpha-\delta+1,\beta-\delta+1,2-\delta;x),\\ \dfrac{\mathrm{d}P(r)}{\mathrm{d}r}=\dfrac{n\alpha\beta x}{\delta}F(\alpha+1,\beta+1,\delta+1;x)+\dfrac{P(r)}{r},\\ \dfrac{\mathrm{d}Q(r)}{\mathrm{d}r}=\dfrac{1}{r}\Big(\dfrac{n(\alpha-\delta+1)(\beta-\delta+1)x}{(2-\delta)r}F(\alpha-\delta+2,\beta-\delta+2,3-\delta;x)-Q(r)\Big).\end{cases} \tag{22}$$

Then, with Eq. (7) and the fifth equation of Eq. (10), the stress components and the perturbation of magnetic field can be derived as

$$\begin{cases} \sigma_r = (\overline{\lambda}+2\overline{G})\Big(C_1\dfrac{\mathrm{d}P(r)}{\mathrm{d}r}+C_2\dfrac{\mathrm{d}Q(r)}{\mathrm{d}r}\Big)+\overline{\lambda}\Big(C_1\dfrac{P(r)}{r}+C_2\dfrac{Q(r)}{r}\Big), \\ \sigma_\theta = \overline{\lambda}\Big(C_1\dfrac{\mathrm{d}P(r)}{\mathrm{d}r}+C_2\dfrac{\mathrm{d}Q(r)}{\mathrm{d}r}\Big)+(\overline{\lambda}+2\overline{G})\Big(C_1\dfrac{P(r)}{r}+C_2\dfrac{Q(r)}{r}\Big), \\ \sigma_z = \overline{\lambda}\Big(C_1\dfrac{\mathrm{d}P(r)}{\mathrm{d}r}+C_2\dfrac{\mathrm{d}Q(r)}{\mathrm{d}r}+C_1\dfrac{P(r)}{r}+C_2\dfrac{Q(r)}{r}\Big), \\ h_z = -H_z\Big(C_1\dfrac{\mathrm{d}P(r)}{\mathrm{d}r}+C_2\dfrac{\mathrm{d}Q(r)}{\mathrm{d}r}+C_1\dfrac{P(r)}{r}+C_2\dfrac{Q(r)}{r}\Big). \end{cases} \tag{23}$$

With the natural boundary conditions $\sigma_r|_{r=a}=-p$ and $\sigma_r|_{r=b}=0$, the following equations are obtained:

$$\begin{cases} C_1 = -p((\overline{\lambda}(b)+2\overline{G}(b))Q'(b)+\overline{\lambda}(b)Q(b)/b)/C_0, \\ C_2 = p((\overline{\lambda}(b)+2\overline{G}(b))P'(b)+\overline{\lambda}(b)P(b)/b)/C_0, \end{cases} \tag{24}$$

where

$$\begin{aligned} C_0 =& ((\overline{\lambda}(b)+2\overline{G}(b))Q'(b)+\overline{\lambda}(b)Q(b)/b)((\overline{\lambda}(a)+2\overline{G}(a))P'(a)+\overline{\lambda}(a)P(a)/a) \\ &-((\overline{\lambda}(a)+2\overline{G}(a))Q'(a)+\overline{\lambda}(a)Q(a)/a)((\overline{\lambda}(b)+2\overline{G}(b))P'(b)+\overline{\lambda}(b)P(b)/b). \end{aligned} \tag{25}$$

In the following, some special situations are discussed.

(a) If $c_0 \neq 0$ and $c_1 = 0$, which indicates that the tube contains only one material with graded parameters along the radial direction, then Eq. (14) reduces to the well-known Eulerian equation,

$$r^2\frac{\mathrm{d}^2u}{\mathrm{d}r^2}+r\frac{\mathrm{d}u}{\mathrm{d}r}-u=0 \tag{26}$$

with the solution as

$$u(r)=\frac{pa^2}{2(b^2-a^2)}\Big(\frac{r}{c_0(\lambda_1+G_1)+(1-c_0)(\lambda_2+G_2)}+\frac{b^2}{r(c_0G_1+(1-c_0)G_2)}\Big), \tag{27}$$

by which Eq. (23) can be rewritten as

$$\begin{cases} \sigma_r = \dfrac{pa^2}{b^2-a^2}\Big(1-\dfrac{b^2}{r^2}\Big), \\ \sigma_\theta = \dfrac{pa^2}{b^2-a^2}\Big(1+\dfrac{b^2}{r^2}\Big), \\ \sigma_z = \dfrac{pa^2(c_0\lambda_1+(1-c_0)\lambda_2)}{(b^2-a^2)(c_0(\lambda_1+G_1)+(1-c_0)(\lambda_2+G_2))}, \\ h_z = -\dfrac{pa^2H_z}{(b^2-a^2)(c_0(\lambda_1+G_1)+(1-c_0)(\lambda_2+G_2))}. \end{cases} \tag{28}$$

(b) If $n=0$, the tube becomes isotropic, and Eqs. (27) and (28) change into the results given by Ref. [55].

Note that, in the above two cases, Lorentz's stress in the radial direction approaches zero which can be verified by taking Eq. (26) into Eq. (11).

(c) If $H_z = 0$ and $c_1 = -c_0 k$, Eqs. (21) and (23) reduce to Eqs. (12) and (13) obtained by Ref. [48].

2.2 Case 2: $\phi_1 = 0$

In this case, Eq. (14) can be simplified as

$$\phi_2 r^2 \frac{\mathrm{d}^2 u}{\mathrm{d}r^2} + \phi_3 r \frac{\mathrm{d}u}{\mathrm{d}r} + \phi_4 u = 0 \tag{29}$$

with the solution

$$u(r) = C_3 r^{m_1} + C_4 r^{m_2}. \tag{30}$$

Then, with the above results, we derive Eq. (23) as

$$\begin{cases} \sigma_r = C_3 r^{m_1-1}((m_1+1)\overline{\lambda} + 2m_1\overline{G}) + C_4 r^{m_2-1}((m_2+1)\overline{\lambda} + 2m_2\overline{G}), \\ \sigma_\theta = C_3 r^{m_1-1}((m_1+1)\overline{\lambda} + 2\overline{G}) + C_4 r^{m_2-1}((m_2+1)\overline{\lambda} + 2\overline{G}), \\ \sigma_z = \overline{\lambda}(C_3(m_1+1)r^{m_1-1} + C_4(m_2+1)r^{m_2-1}), \\ h_z = -H_z(C_3(m_1+1)r^{m_1-1} + C_4(m_2+1)r^{m_2-1}), \end{cases} \tag{31}$$

where $m_1 = \frac{1}{2} - \frac{\phi_3}{2\phi_2} + \frac{1}{2}\sqrt{\left(\frac{\phi_3}{\phi_2} - 1\right)^2 - \frac{4\phi_4}{\phi_2}}$, $m_2 = \frac{1}{2} - \frac{\phi_3}{2\phi_2} - \frac{1}{2}\sqrt{\left(\frac{\phi_3}{\phi_2} - 1\right)^2 - \frac{4\phi_4}{\phi_2}}$, and C_3 and C_4 given by the boundary conditions $\sigma_r|_{r=a} = -p$ and $\sigma_r|_{r=b} = 0$ are

$$\begin{cases} C_3 = -pb^{m_2-1}((m_2+1)\overline{\lambda}(b) + 2m_2\overline{G}(b))/\overline{C}_0, \\ C_4 = pb^{m_1-1}((m_1+1)\overline{\lambda}(b) + 2m_1\overline{G}(b))/\overline{C}_0, \end{cases} \tag{32}$$

where

$$\begin{aligned} \overline{C}_0 = {} & a^{m_1-1}b^{m_2-1}((m_1+1)\overline{\lambda}(a) + 2m_1\overline{G}(a))((m_2+1)\overline{\lambda}(b) + 2m_2\overline{G}(b)) \\ & - a^{m_2-1}b^{m_1-1}((m_1+1)\overline{\lambda}(b) + 2m_1\overline{G}(b))((m_2+1)\overline{\lambda}(a) + 2m_2\overline{G}(a)). \end{aligned} \tag{33}$$

Therefore, we have some special situations as follows.

(a) When the material A and the material B have the same Poisson's ratio and conditions as $E_2 - E_1 = E_0, E_2/E_0 = c_0, m_2 - m_1 = m_0, m_2/m_0 = c_0$, and $c_1 = -1$, Eq. (29) reduces to Eq. (4) in Ref. [42], i.e.,

$$r^2 \frac{\mathrm{d}^2 u}{\mathrm{d}r^2} + (1 + \overline{\zeta} n) r \frac{\mathrm{d}u}{\mathrm{d}r} + (\overline{\eta} n - 1)u = 0, \tag{34}$$

where

$$\begin{cases} \overline{\zeta} = \dfrac{(E_2 - E_1)(1-v)}{(E_2 - E_1)(1-v) + H_z^2(\mu_2 - \mu_1)(1+v)(1-2v)}, \\ \overline{\eta} = \dfrac{(E_2 - E_1)v}{(E_2 - E_1)(1-v) + H_z^2(\mu_2 - \mu_1)(1+v)(1-2v)}. \end{cases} \tag{35}$$

(b) When $H_z = 0$, Eq. (34) takes a similar form to that in Ref. [10], i.e.,

$$r^2 \frac{\mathrm{d}^2 u}{\mathrm{d}r^2} + (1+n) r \frac{\mathrm{d}u}{\mathrm{d}r} + \left(\frac{nv}{1-v} - 1\right) u = 0. \tag{36}$$

Then, the same solutions for the displacement and stress components can be determined.

3 Numerical examples and discussion

With the use of the following dimensionless quantities $\overline{r} = r/b$, $\overline{a} = a/b$, $\overline{\sigma}_r = \sigma_r/p$, $\overline{\sigma}_\theta = \sigma_\theta/p$, $\overline{\sigma}_z = \sigma_z/p$, $\overline{u} = u(r)E_2/(bp)$, and $\overline{h}_z = h_z(r)E_2/(H_z p)$, where a and b are the inner and outer radii, respectively, p is the internal pressure, H_z is the magnetic intensity, and E_2 is the elastic modulus of the material B, this numerical part provides some examples to explore the influences of Poisson's ratio, the magnetic density, and the index n. Moreover, the selected configuration and material parameters are listed in Table 1.

Table 1 Selected configuration and material parameters

$\overline{a}$	c_0	c_1	E_1/GPa	E_2/GPa	$\mu/(\mathrm{H\cdot m^{-1}})$
0.7	1	1	210	70	$4\pi \times 10^{-7}$

3.1 Effects of Poisson's ratio

In this part, effects of Poisson's ratio on the FGM tube in uniform magnetic fields have been discussed. It is assumed that the FGM tube is made by two different materials, and three sets of Poisson's ratios are chosen, i.e., $v_1 = 0.3$, $v_2 = 0.2$; $v_1 = v_2 = 0.3$; and $v_1 = 0.3$, $v_2 = 0.4$.

Indicated from Fig. 2, it can be concluded that Poisson's ratio has an obvious effect on the distribution of the radial displacement for the FGM tube under the uniform magnetic field compared with the results[48] without magnetic fields. Aside from the displacement, Poisson's ratio displays the similar effects on stress components, as shown in Figs. 3–5. Specifically, the trend of the distribution of radial stress increases with the decrease of Poisson's ratio, which is contrary to the circumferential stress (see Figs. 3 and 4). As for the axial stress, the influence of Poisson's ratio is more pronounced, which is closer to the inner tube's surface. Meanwhile, the minimum value achieves in the outer surface as exhibited in Fig. 5.

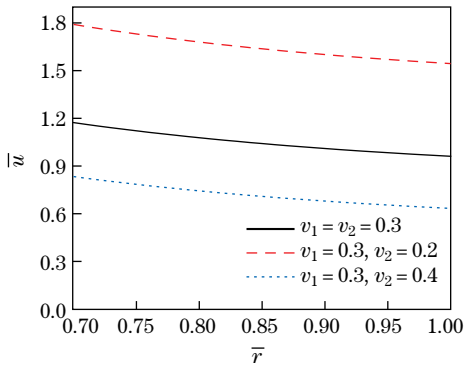

Fig. 2 Evolutions of the radial displacement with different Poisson's ratios ($n = 1.5$, $H_z = 2.23 \times 10^9$ A/m)

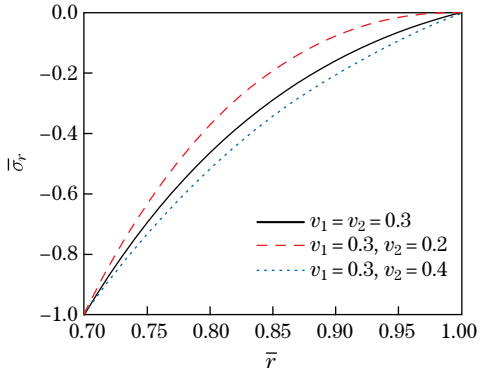

Fig. 3 Evolutions of the radial stress with different Poisson's ratios ($n = 1.5$, $H_z = 2.23 \times 10^9$ A/m)

From Fig. 6, it can be seen that the magnetic field vector distributes almost horizontally for each set of chosen Poisson's ratio while all the values are negative.

3.2 Effects of the magnetic intensity

Based on Eqs. (21), (23), (30), and (31), this part investigates the effects of magnetic intensity on the mechanical responses of the FGMs tube and makes comparisons with the situation ignoring the magnetic field. All the results have been graphed in Figs. 7–9.

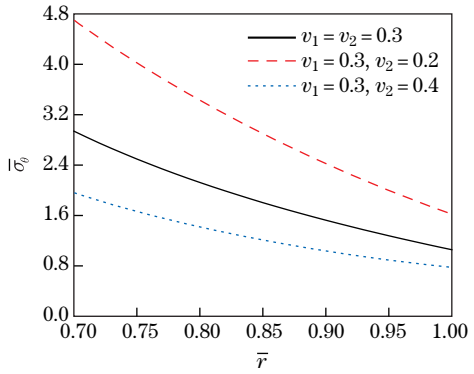

Fig. 4 Evolutions of the circumferential stress with different Poisson's ratios ($n = 1.5$, $H_z = 2.23 \times 10^9$ A/m)

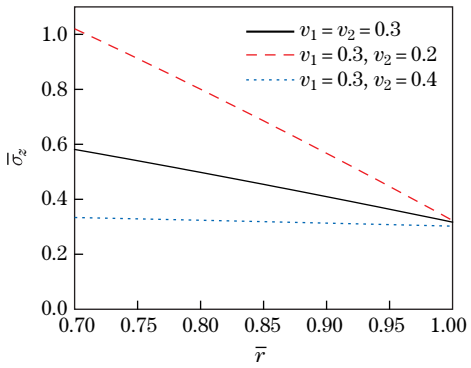

Fig. 5 Evolutions of the axial stress with different Poisson's ratios ($n = 1.5$, $H_z = 2.23 \times 10^9$ A/m)

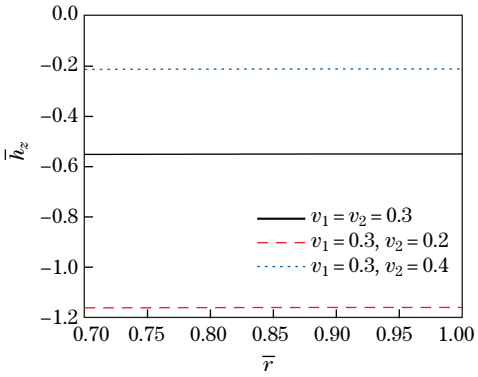

Fig. 6 Evolutions of the perturbation of magnetic field with different Poisson's ratios ($n = 1.5$, $H_z = 2.23 \times 10^9$ A/m)

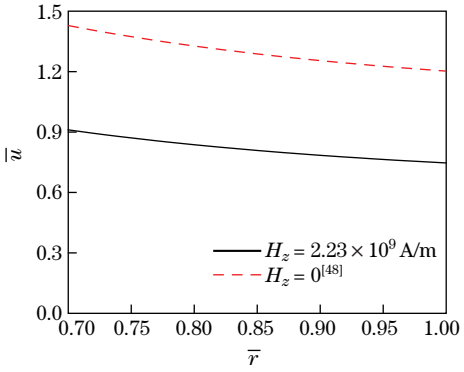

Fig. 7 Comparisons of two different magnetic intensities ($H_z = 2.23 \times 10^9$ A/m in this work and $H_z = 0$[48]) for the radial displacement ($n = 1.5$, $v_1 = 0.2$, $v_2 = 0.3$)

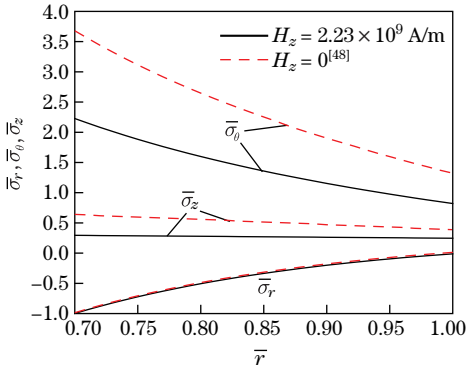

Fig. 8 Comparisons of two different magnetic intensities ($H_z = 2.23 \times 10^9$ A/m in this work and $H_z = 0$[48]) for the stresses ($n = 1.5$, $v_1 = 0.2$, $v_2 = 0.3$)

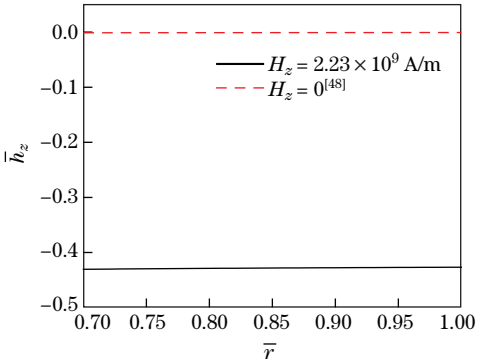

Fig. 9 Comparisons of two different magnetic intensities ($H_z = 2.23 \times 10^9$ A/m in this work and $H_z = 0$[48]) for the perturbation of magnetic field ($n = 1.5$, $v_1 = 0.2$, $v_2 = 0.3$)

As illustrated in Fig. 7, the radial displacement of the cases with/without the magnetic field, declines from the inner surface to the outer surface, while the differences are verified by the larger radial displacement when $H_z = 0$ than that when $H_z = 2.23 \times 10^9$ A/m. Figure 8 shows the evident distribution trends among the axial, radial, and circumferential stresses, while the value of the radial stress increases with the increment of radius, and the other two just decrease. For different magnetic intensities, the radial stress keeps nearly unchanged but certain differences happen to the stresses in the axial and circumferential directions. From Fig. 9, it can be acknowledged that the magnetic field affects the perturbation of magnetic vector significantly. For example, when there is no magnetic field, the perturbation of magnetic vector is equal to zero, while it weakly increases along the radial direction for the case of the magnetic field with a certain intensity.

3.3 Effects of the parameter n

Since the volume fractions of the materials A and B are determined by the parameter n as shown in Eq. (1), it seems rather necessary to detect its impacts on the performance of the FGM tube (see Figs. 10–14). In this section, the parameters are selected as $n = 1.5, 3.0$, and 5.0.

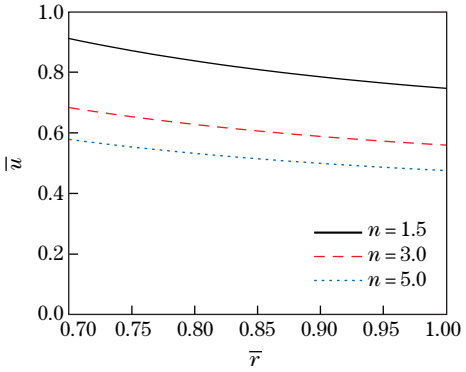

Fig. 10 Evolutions of the radial displacement with different values of the parameter n ($v_1 = 0.2$, $v_2 = 0.3$, $H_z = 2.23 \times 10^9$ A/m)

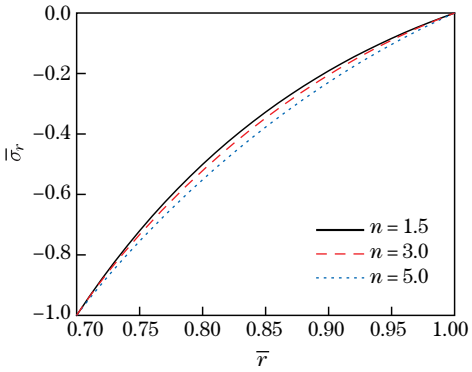

Fig. 11 Evolutions of the radial stress with different values of the parameter n ($v_1 = 0.2$, $v_2 = 0.3$, $H_z = 2.23 \times 10^9$ A/m)

Figure 10 shows that the radial displacement declines with the increment of the parameter n and reaches its minimum value at the outer surface. For the distribution of stress components with the natural boundary conditions $\overline{\sigma}_r|_{\overline{r}=\overline{a}} = 0$ and $\overline{\sigma}_r|_{\overline{r}=\overline{b}} = 0$, the parameter n just

inconsiderably influences the distribution of the radial stress, i.e., the differences mainly focus on the middle part of the tube with a less than 3% accretion from $n = 1.5$ to $n = 3$ while a less than 3.5% increment from $n = 3$ to $n = 5$ (see Fig. 11). For the stresses in the circumferential and axial directions, the maximum difference (more than 50%) is located at the outer surface when the parameter n changes from 3 to 5 (see Figs. 12 and 13). As shown in Fig. 14, the distribution of the perturbation of the magnetic field vector is similar to that in Fig. 6. All of these lines are below zero, which can also be easily known from the fifth equation of Eq. (10), and the perturbation of the magnetic field vector will incline to zero with the growth of the parameter n.

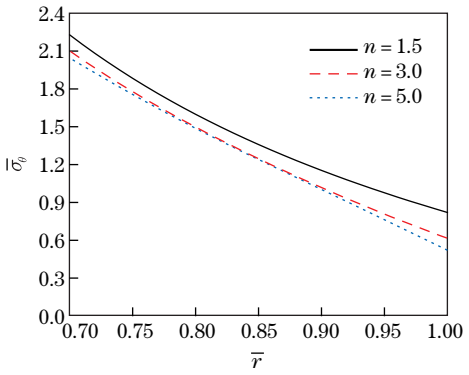

Fig. 12 Evolutions of the circumferential stress with different values of the parameter n ($v_1 = 0.2$, $v_2 = 0.3$, $H_z = 2.23 \times 10^9$ A/m)

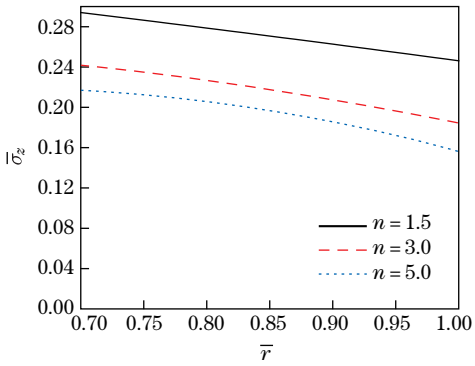

Fig. 13 Evolutions of the axial stress with different values of the parameter n ($v_1 = 0.2$, $v_2 = 0.3$, $H_z = 2.23 \times 10^9$ A/m)

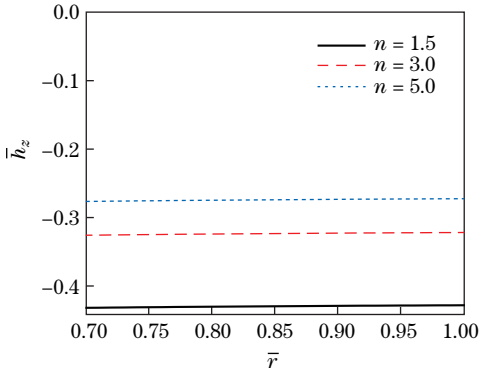

Fig. 14 Evolutions of the perturbation of magnetic field with different values of the parameter n ($v_1 = 0.2$, $v_2 = 0.3$, $H_z = 2.23 \times 10^9$ A/m)

4 Conclusions

In summary, this paper studies the mechanical response of an inner pressurized FGM cylinder composed of two materials within uniform magnetic fields. By assuming the volume fraction of material component as an exponential function form, we derive the analytical expressions of the radial displacement, the stress components, and the perturbation magnetic vector with the Voigt method. Furthermore, the effects of Poisson's ratio, the magnetic intensity, and the parameter n are discussed. From the results of the numerical part, it can be concluded that

both Poisson's ratio and the parameter n have effects on the radial displacement, the axial stress, and the perturbation of the magnetic field vector. Moreover, by comparing the results with those in our previous work, essential differences of the mechanical responses of the FGM tube are illustrated between the situation with and without the action of the magnetic field. These results obtained in this paper can serve as an important contribution to the design and development of the FGM structures within multi-physical fields.

References

[1] MIYAMOTO, Y., KAYSSER, W., RABIN, B., KAWASAKI, A., and FORD, R. G. *Functionally Graded Materials*: *Design*, *Processing and Applications*, Springer Science and Business Media, United States (2013)

[2] DAI, H. L., RAO, Y. N., and DAI, T. A review of recent researches on FGM cylindrical structures under coupled physical interactions, 2000–2015. *Composite Structures*, **152**, 199–225 (2016)

[3] YANG, S. and CHEN, Y. C. Wrinkle surface instability of an inhomogeneous elastic block with graded stiffness. *Proceedings of the Royal Society A Mathematical Physical & Engineering Sciences*, **473**, 20160882 (2017)

[4] JHA, D., KANT, T., and SINGH, R. A critical review of recent research on functionally graded plates. *Composite Structures*, **96**, 833–849 (2013)

[5] GUPTA, A. and TALHA, M. Recent development in modeling and analysis of functionally graded materials and structures. *Progress in Aerospace Sciences*, **79**, 1–14 (2015)

[6] ZHENG, G., PANG, T., SUN, G., WU, S., and LI, Q. Theoretical, numerical, and experimental study on laterally variable thickness (LVT) multi-cell tubes for crashworthiness. *International Journal of Mechanical Sciences*, **118**, 283–297 (2016)

[7] SUN, G., PANG, T., XU, C., ZHENG, G., and SONG, J. Energy absorption mechanics for variable thickness thin-walled structures. *Thin-Walled Structures*, **118**, 214–228 (2017)

[8] SUN, G., TIAN, J., LIU, T., YAN, X., and HUANG, X. Crashworthiness optimization of automotive parts with tailor rolled blank. *Engineering Structures*, **169**, 201–215 (2018)

[9] YOU, L., ZHANG, J., and YOU, X. Elastic analysis of internally pressurized thick-walled spherical pressure vessels of functionally graded materials. *International Journal of Pressure Vessels and Piping*, **82**, 347–354 (2005)

[10] TUTUNCU, N. and OZTURK, M. Exact solutions for stresses in functionally graded pressure vessels. *Composites Part B*: *Engineering*, **32**, 683–686 (2001)

[11] SHI, Z., ZHANG, T., and XIANG, H. Exact solutions of heterogeneous elastic hollow cylinders. *Composite Structures*, **79**, 140–147 (2007)

[12] CHEN, Y. and LIN, X. Elastic analysis for thick cylinders and spherical pressure vessels made of functionally graded materials. *Computational Materials Science*, **44**, 581–587 (2008)

[13] LI, X. F. and PENG, X. L. A pressurized functionally graded hollow cylinder with arbitrarily varying material properties. *Journal of Elasticity*, **96**, 81–95 (2009)

[14] SOFIYEV, A. H. and SCHNACK, E. The stability of functionally graded cylindrical shells under linearly increasing dynamic torsional loading. *Engineering Structures*, **26**, 1321–1331 (2004)

[15] SBURLATI, R. Analytical elastic solutions for pressurized hollow cylinders with internal functionally graded coatings. *Composite Structures*, **94**, 3592–3600 (2012)

[16] ODENBACH, S. Recent progress in magnetic fluid research. *Journal of Physics Condensed Matter*, **16**, 1135–1150 (2004)

[17] RAMANUJAN, R. V. and LAO, L. L. The mechanical behavior of smart magnet-hydrogel composites. *Smart Materials & Structures*, **15**, 952–956 (2006)

[18] CHERTOVICH, A. V., STEPANOV, G. V., KRAMARENKO, E. Y., and KHOKHLOV, A. R. New composite elastomers with giant magnetic response. *Macromolecular Materials & Engineering*, **295**, 336–341 (2010)

[19] BICA, I. The influence of the magnetic field on the elastic properties of anisotropic magnetorheological elastomers. *Journal of Industrial & Engineering Chemistry*, **18**, 1666–1669 (2012)

[20] REDDY, S. K., SURI, A., and MISRA, A. Influence of magnetic field on the compressive behavior of carbon nanotube with magnetic nanoparticles. *Applied Physics Letters*, **102**, 241919 (2013)

[21] PONNUSAMY, P. and AMUTHALAKSHMI, A. Influence of thermal and longitudinal magnetic field on vibration response of a fluid conveying double walled carbon nanotube embedded in an elastic medium. *Journal of Computational & Theoretical Nanoscience*, **11**, 2570–2577 (2014)

[22] ANSARI, R., HASRATI, E., GHOLAMI, R., and SADEGHI, F. Nonlinear analysis of forced vibration of nonlocal third-order shear deformable beam model of magneto-electro-thermo elastic nanobeams. *Composites Part B*: *Engineering*, **83**, 226–241 (2015)

[23] EBRAHIMI, F. and REZA, M. Magnetic field effects on buckling behavior of smart size-dependent graded nanoscale beams. *European Physical Journal Plus*, **131**(7), 238 (2016)

[24] ESPINOSA-ALMEYDA, Y., CAMACHO-MONTES, H., RODRÍGUEZ-RAMOS, R., GUINOVART-DÍAZ, R., LÓPEZ-REALPOZO, J. C., BRAVO-CASTILLERO, J., and SABINA, F. J. Influence of imperfect interface and fiber distribution on the antiplane effective magneto-electro-elastic properties for fiber reinforced composites. *International Journal of Solids and Structures*, **112**, 155–168 (2017)

[25] DANIEL, L., HUBERT, O., BUIRON, N., and BILLARDON, R. Reversible magneto-elastic behavior: a multiscale approach. *Journal of the Mechanics & Physics of Solids*, **56**, 1018–1042 (2008)

[26] YANG, S., ZHAO, X., and SHARMA, P. Revisiting the instability and bifurcation behavior of soft dielectrics. *Journal of Applied Mechanics*, **84**(3), 031008 (2017)

[27] YANG, S., ZHAO, X., and SHARMA, P. Avoiding the pull-in instability of a dielectric elastomer film and the potential for increased actuation and energy harvesting. *Soft Matter*, **13**, 4552–4558 (2017)

[28] ALAMEH, Z., YANG, S., DENG, Q., and SHARMA, P. Emergent magnetoelectricity in soft materials, instability, and wireless energy harvesting. *Soft Matter* (2018) DOI: 10.1039/C8SM00587G

[29] VARGA, Z., FILIPCSEI, G., and ZRÍNYI, M. Magnetic field sensitive functional elastomers with tuneable elastic modulus. *Polymer*, **47**, 227–233 (2006)

[30] STEPANOV, G. V., ABRAMCHUK, S. S., GRISHIN, D. A., NIKITIN, L. V., KRAMARENKO, E. Y., and KHOKHLOV, A. R. Effect of a homogeneous magnetic field on the viscoelastic behavior of magnetic elastomers. *Polymer*, **48**, 488–495 (2007)

[31] KRAMARENKO, E. Y., CHERTOVICH, A. V., STEPANOV, G. V., SEMISALOVA, A. S., MAKAROVA, L. A., PEROV, N. S., and KHOKHLOV, A. R. Magnetic and viscoelastic response of elastomers with hard magnetic filler. *Smart Materials and Structures*, **24**, 035002 (2015)

[32] DAI, H. and WANG, X. Dynamic responses of piezoelectric hollow cylinders in an axial magnetic field. *International Journal of Solids and Structures*, **41**, 5231–5246 (2004)

[33] DAI, H. and WANG, X. Magneto-thermo-electro-elastic transient response in a piezoelectric hollow cylinder subjected to complex loadings. *International Journal of Solids and Structures*, **43**, 5628–5646 (2006)

[34] DAI, H. and WANG, X. The dynamic response and perturbation of magnetic field vector of orthotropic cylinders under various shock loads. *International Journal of Pressure Vessels and Piping*, **83**, 55–62 (2006)

[35] AREFI, M., RAHIMI, G., and KHOSHGOFTAR, M. Exact solution of a thick walled functionally graded piezoelectric cylinder under mechanical, thermal and electrical loads in the magnetic field. *Smart Structures and Systems*, **9**, 427–439 (2012)

[36] DAI, H., FU, Y., and YANG, J. Electromagnetoelastic behaviors of functionally graded piezoelectric solid cylinder and sphere. *Acta Mechanica Sinica*, **23**, 55–63 (2007)

[37] DAI, H. and FU, Y. Magnetothermoelastic interactions in hollow structures of functionally graded material subjected to mechanical loads. *International Journal of Pressure Vessels and Piping*, **84**, 132–138 (2007)

[38] BAYAT, M., RAHIMI, M., SALEEM, M., MOHAZZAB, A., WUDTKE, I., and TALEBI, H. One-dimensional analysis for magneto-thermo-mechanical response in a functionally graded annular variable-thickness rotating disk. *Applied Mathematical Modelling*, **38**, 4625–4639 (2014)

[39] DAI, H. L., HONG, L., FU, Y. M., and XIAO, X. Analytical solution for electromagnetothermoelastic behaviors of a functionally graded piezoelectric hollow cylinder. *Applied Mathematical Modelling*, **34**, 343–357 (2010)

[40] DAI, H. L., RAO, Y. N., and JIANG, H. J. An analytical method for magnetothermoelastic analysis of functionally graded hollow cylinders. *Applied and Computational Mathematics*, **218**, 1467–1477 (2011)

[41] DAI, H., FU, Y., and DONG, Z. Exact solutions for functionally graded pressure vessels in a uniform magnetic field. *International Journal of Solids and Structures*, **43**, 5570–5580 (2006)

[42] AKBARI, M. and GHANBARI, J. Discussion on "Exact solutions for functionally graded pressure vessels in a uniform magnetic field". *International Journal of Solids and Structures*, **78**, 216–218 (2016)

[43] ARANI, A. G., LOGHMAN, A., SHAJARI, A., and AMIR, S. Semi-analytical solution of magneto-thermo-elastic stresses for functionally graded variable thickness rotating disks. *Journal of Mechanical Science and Technology*, **24**, 2107–2118 (2010)

[44] ARANI, A. G., AZAMIA, M., and SEPIANI, H. Magneto-thermo-elastic stresses and perturbation of the magnetic field vector in an EGM rotating disk. *Journal of Solid Mechanics*, **2**, 168–178 (2010)

[45] ARANI, A. G. and AMIR, S. Magneto-thermo-elastic stresses and perturbation of magnetic field vector in a thin functionally graded rotating disk. *Journal of Solid Mechanics*, **3**, 392–407 (2011)

[46] SAADATFAR, M. and AGHAIE, M. Thermoelastic analysis of a rotating functionally graded cylindrical shell with functionally graded sensor and actuator layers on an elastic foundation placed in a constant magnetic field. *Journal of Intelligent Material Systems and Structures*, **27**, 512–527 (2016)

[47] XIN, L., LU, W., YANG, S., JU, C., and DUI, G. Influence of linear work hardening on the elastic-plastic behavior of a functionally graded thick-walled tube. *Acta Mechanica*, **227**, 2305–2321 (2016)

[48] XIN, L., DUI, G., YANG, S., and ZHANG, J. An elasticity solution for functionally graded thick-walled tube subjected to internal pressure. *International Journal of Mechanical Sciences*, **89**, 344–349 (2014)

[49] XIN, L., YANG, S., ZHOU, D., and DUI, G. An approximate analytical solution based on the Mori-Tanaka method for functionally graded thick-walled tube subjected to internal pressure. *Composite Structures*, **135**, 74–82 (2016)

[50] XIN, L., DUI, G., YANG, S., and ZHOU, D. Solutions for behavior of a functionally graded thick-walled tube subjected to mechanical and thermal loads. *International Journal of Mechanical Sciences*, **98**, 70–79 (2015)

[51] QU, J. M. and CHERKAOUI, M. *Fundamentals of Micromechanics of Solids*, John Wiley & Sons, New Jersey (2006)

[52] LI, S. and GAO, X. L. *Handbook of Micromechanics and Nanomechanics*, CRC Press, Singapore (2013)

[53] LI, S. and WANG, G. *Introduction to Micromechanics and Nanomechanics*, World Scientific Publishing Company, New Jersey (2008)

[54] KAMKE, E. *Manual of Ordinary Differential Equations*, Science Press, Beijing (1978)

[55] TIMOSHENKO, S. P. and GOODIER, J. N. *Theory of Elasticity*, 3rd ed., McGraw-Hill, New York (1970)